CREEP DEFORMATION AND RUPTURE BEHAVIOUR OF THE MONOCRYSTALLINE SUPERALLOY CMSX-4 — A COMPARISON WITH THE ALLOY SRR 99.

W. Schneider[1)], J. Hammer[2)] and H. Mughrabi[1)].

[1)]Institut für Werkstoffwissenschaften, Universität Erlangen-Nürnberg,

D-W 8520 Erlangen, F. R. Germany.

[2)]Eurocopter, D-W 8000 München 80, F. R. Germany.

Abstract

Monocrystalline specimens of the γ'-hardened Rhenium-containing superalloy CMSX-4 were tested in tensile creep under constant stress at temperatures of 800°C and 950°C. The shapes of the differentiated creep curves are distinctly different for the two temperatures. All curves exhibit minima of the creep rate and a subsequent increase, in particular at low stresses and high temperatures, due to the formation of the γ/γ'-raft structure. The latter was found to deteriorate the creep properties under the given test conditions. The creep rupture behaviour can be described in a modified creep rupture diagram, based on the threshold stress concept. According to a Larson-Miller plot, the alloy CMSX-4 offers an improved creep temperature capability, compared to SRR 99, of about 20°C at low stresses and more than 40°C at higher stresses.

Superalloys 1992
Edited by S.D. Antolovich, R.W. Stusrud, R.A. MacKay,
D.L. Anton, T. Khan, R.D. Kissinger, D.L. Klarstrom
The Minerals, Metals & Materials Society, 1992

Introduction, Objectives

High-temperature nickel-base superalloys are important materials for gas turbine applications. Modern monocrystalline nickel-base superalloys have been developed in order to remove grain boundary strengthening elements and to raise the incipient melting temperature. This allows heat treatments at higher temperatures, whereby material homogeneity is improved and the coarse primary γ'-particles associated with the γ/γ' eutectic are dissolved. The orientations of monocrystalline turbine blades lie near a $\langle 001 \rangle$ direction. This provides the best combination of properties at intermediate and high temperatures [1].
Further improvement of the creep behaviour of superalloys was achieved by specific selection of alloy composition. For example, Rhenium appears to be becoming increasingly important as an alloying element in single crystal superalloys, making the material more resistant by strenghtening of the γ-matrix and by reduction of the γ' coarsening rate [2-5].
In this paper, the results of an investigation which is still under way on the creep deformation and rupture behaviour of the second generation Rhenium-containing monocrystalline superalloy CMSX-4 are reported. The results are compared with results obtained in an already completed extensive study on the monocrystalline superalloy SRR 99 [6, 7].

Material Characterisation and Experimental Procedures

Samples

Single crystal specimens of CMSX-4 and SRR 99 were provided in the form of cast rods, with longitudinal orientations within 10° of [001]. The exact orientations of the specimen axes were determined by the Laue back-reflection technique. The chemical composition of CMSX-4 is listed in Table I.

Table I: Chemical composition of CMSX-4 (wt.-%)

Cr	Al	Ti	Mo	W	Ta	Co	Re	Hf	Ni
6.4	5.7	1.0	0.6	6.3	6.5	9.5	2.9	0.1	bal.

The main difference in the chemistries of CMSX-4 and SRR 99 is the addition of approximately 3% Rhenium. CMSX-4 also contains higher levels of refractory elements such as Mo, W and Ta.
The heat treatment of CMSX-4 consists of a two-step solution treatment followed by a two-step ageing treatment. The final microstructure consists of approximately 70 vol% cuboidal γ'-precipitates with average edge lengths of 0.47µm. Extraction replicas revealed the presence of spherical secondary γ'-precipitates with an average diameter of 40nm. No interfacial dislocations were present, presumably because of the small γ/γ' misfit δ (δ=-2.4·10^{-3}). Grown-in dislocations were seen both in regions with irregularly shaped γ'-precipitates and at subgrain boundaries. These areas are widely spaced in a similar fashion as reported in [8]. Inside the γ'-precipitates no dislocations were found.

Creep tests

CMSX-4 specimens with a gage length of 30mm and a diameter of 6mm were prepared by mechanical machining and grinding. Prior to mechanical testing all samples were polished electrochemically. These specimens were tested in tensile creep under constant stress at temperatures of 800°C and 950°C. The temperature control was better than ±0.5°C. The applied stress varied between 241 MPa and 925 MPa. The total strain was measured with a linear variable differential transformer. The strain resolution of the system was better than 10^{-5}. Using the temperature-dependent elastic constants of CMSX-4 which were measured with a resonance system as in [9], the elastic strains were calculated for all specimens, taking

into account their specific orientations. Thus the plastic strains ε_{pl} could be obtained. All strain data reported subsequently refer to the plastic strains.

Microstructural observations

The γ/γ' microstructure and the dislocation distribution of the specimens in the initial state and after high-temperature creep were investigated by light optical, transmission electron microscopy (TEM) and scanning electron microscopy (SEM).

Creep Behaviour and Microstructural Changes

Typical creep curves obtained at the testing temperatures T=800°C and T=950°C are shown in Fig. 1. The differentiated creep curves, plotted as plastic strain rate $\dot{\varepsilon}_{pl}$ versus plastic strain ε_{pl} (Fig. 1b, 1d), offer several advantages [10] compared to the more common ε_{pl} vs. time t plots (Fig. 1a, 1c): 1) It is straightforward to distinguish (in more detail) the different stages of creep, 2) the exact value of the minimum plastic creep rate $\dot{\varepsilon}_{min}$ which must be known for a more detailed description of the creep behaviour can be determined directly.
Independent of the applied stress and the temperature, the alloy CMSX-4 shows no incubation period before the creep strain develops. This is in contrast to other work on monocrystalline superalloys, cf. for example [8, 11]. At the testing temperature T=800°C the observed creep curves are similar and show an unusual course. Primary transient creep can be divided into three regions. In region 1 the creep rate decreases until it passes through a

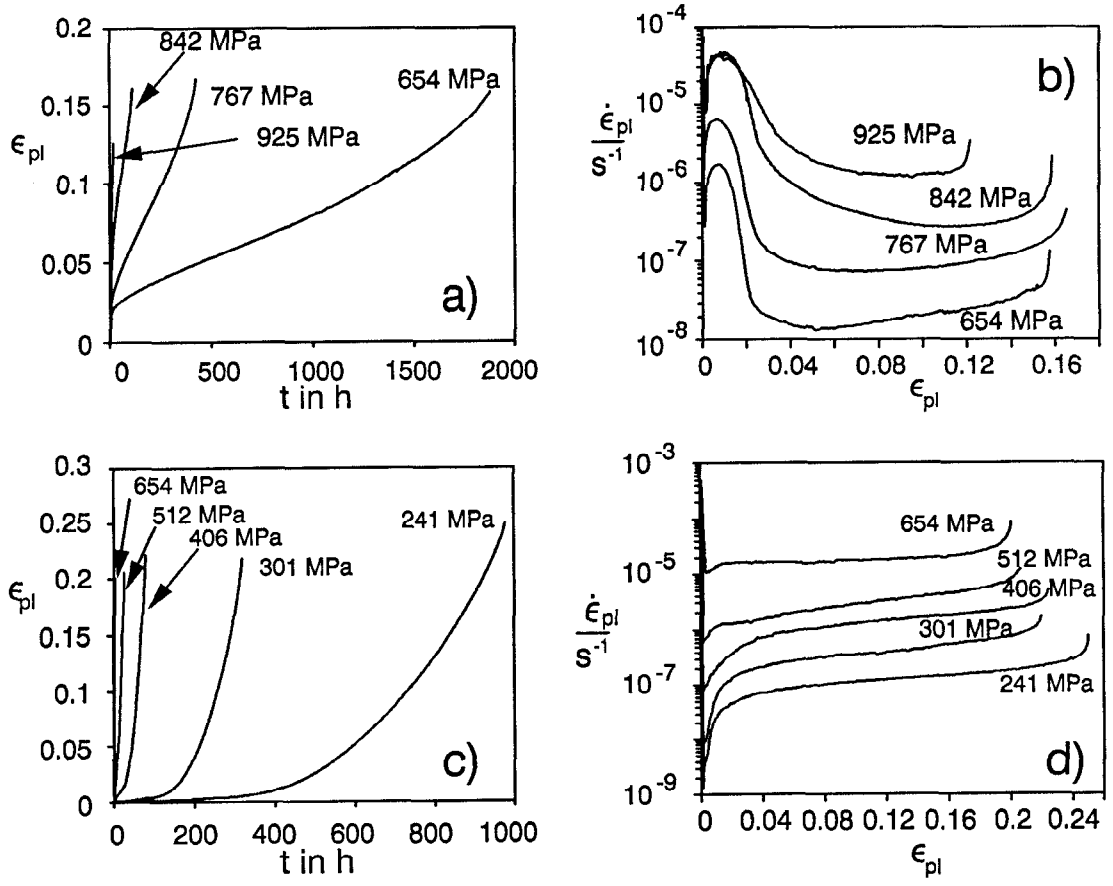

Figure 1: Typical creep curves. (a) and (c) Plots of strain ε_{pl} vs. time t at 800°C and 950°C, respectively. (b) and (d) differentiated creep curves: creep strain rate $\dot{\varepsilon}_{pl}$ vs. plastic strain ε_{pl} at 800°C and 950°C, respectively.

local minimum. At this point, region 2 starts with an increasing creep rate, followed, after attainment of a local maximum, by region 3 with once again decreasing creep rate. Under these test conditions no constant steady-state creep rate is attained and the second minimum of the creep rate is shifted towards higher strains with increasing stress. The investigation of the microstructural changes during creep at T=800°C show that even after long time exposure no changes in the γ'-morphology occur (Fig. 2a).

At the testing temperature T=950°C (Fig. 1c, 1d) primary creep occurs as normal transient creep, i.e. the creep rate decreases sharply with increasing strain. After very small amounts of plastic strain a minimum of the creep rate $\dot{\varepsilon}_{min}$ is attained. With increasing strain the creep rate also increases until the creep curve passes into an almost horizontal region. Generally this nearly horizontal course of the creep rate is no true steady-state region because the creep rate continues to increase within this region. This creep acceleration is accounted for by a dynamic strain-softening process as proposed by Dyson and McLean [12]. The increase of the creep rate shortly after $\dot{\varepsilon}_{min}$ is attained is more pronounced for low stresses, due to the formation of the γ/γ'-raft structure. Interrupted creep tests show that, in all cases investigated so far, no morphological changes had occurred till the point of minimum creep rate. It was, however, verified that after the subsequent increase of the creep rate till the creep curves merge into the nearly horizontal "plateau-like" region, the transition of initially cuboidal γ'-precipitates to the raft structure is completed. In contrast to the deformation at 800°C, deformation at 950°C under low stresses (σ≤406 MPa) results in a fully developed γ/γ'-raft structure which is aligned normal to the stress axis (Fig. 2b), as expected for negative misfit. Creep curves of monocrystalline SRR 99 at 750°C and 900°C are similar to those of CMSX-4 at 800°C and 950°C, respectively, cf. Fig 1. In contrast to creep of CMSX-4, creep of SRR 99 at the lower temperature leads to an almost steady-state creep rate. After fracture at T=750°C and independent of the applied stress the microstructure still consists of the initially cuboidal γ'-precipitates. Creep at the higher testing temperature T=900°C and for σ≤444 MPa leads to the formation of the γ/γ'-raft structure. More details are found in [6, 7].

Fig. 3 shows TEM micrographs of CMSX-4 specimens deformed at T=800°C and different stresses. At the low stress σ=654 MPa (Fig. 3a), the use of the stereo imaging technique reveals that nearly all dislocations are in γ-matrix channels and are located at the γ/γ' interface. It is evident that the interfacial dislocation networks are much more pronounced at the γ/γ' interfaces which are perpendicular to the stress axis than at those which are parallel to the stress axis. This observation reflects the fact that the deformation by dislocation glide is most pronounced in the γ-channels which lie perpendicular to the stress axis and in which the internal (coherency) stresses aid the tensile deformation, whereas they oppose it in the γ-channels which lie parallel to the stress axis [8, 13, 14]. Stacking faults are seen clearly and are found to lie within the γ'-precipitates. At the highest stress σ=925 MPa (Fig. 3b), the

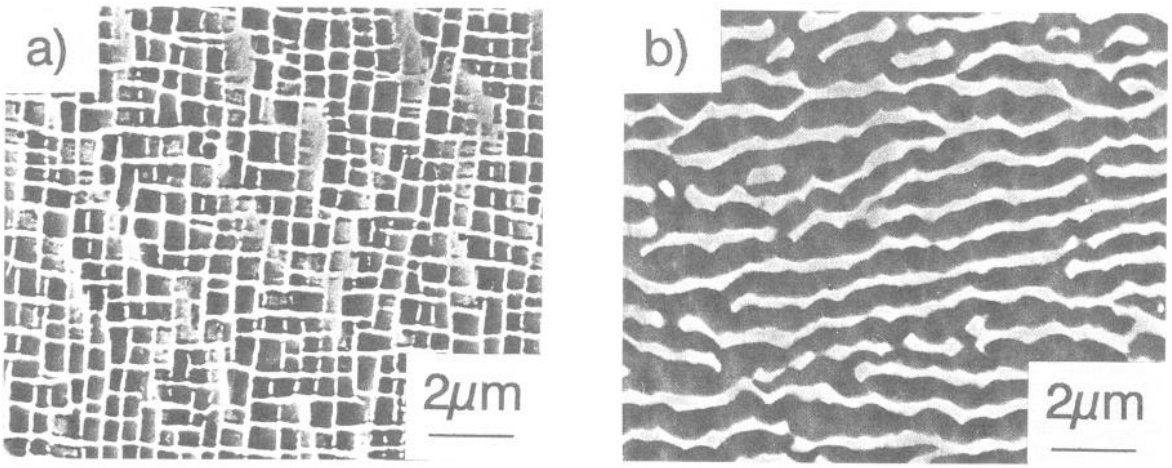

Figure 2: SEM micrographs showing the γ'-morphology of crystals crept till rupture. (a) T=800°C, σ=654 MPa. (b) T=950°C, σ=301 MPa. Stress axis is vertical.

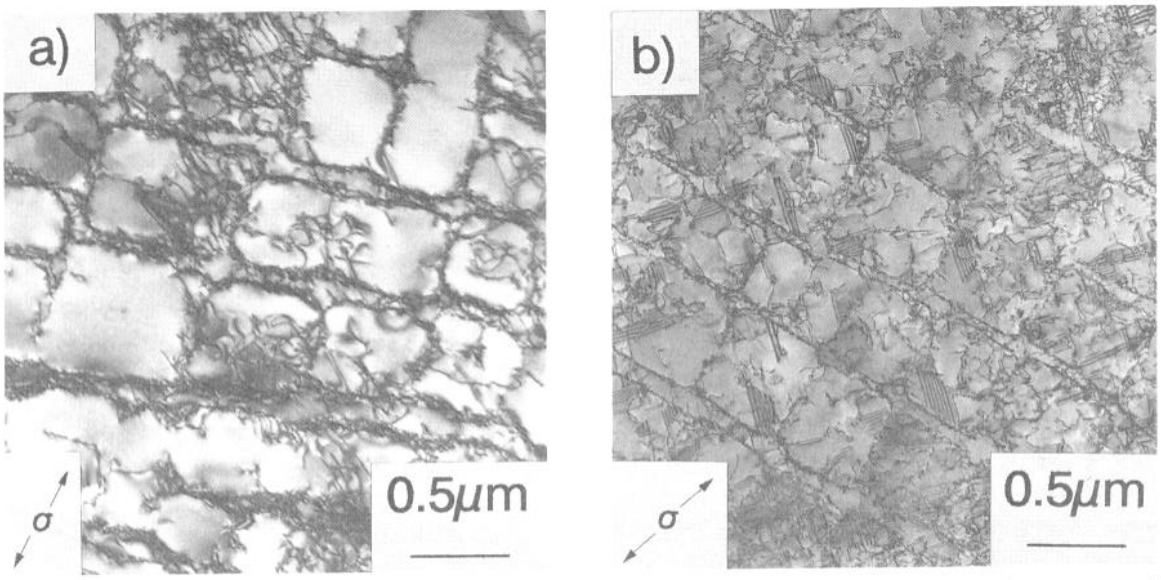

Figure 3: TEM micrographs showing the typical dislocation microstructures after creep till rupture at T=800°C. (a) σ=654 MPa. (b) σ=925 MPa. (100) foils, parallel to stress axis [001].

density of stacking faults has increased. Stereo pairs show that all stacking faults are within γ'-precipitates. The high density of stacking faults at T=800°C suggests that cutting of γ'-precipitates plays an important role in deformation under these test conditions as discussed in [15, 16].

The microstructure of CMSX-4 tested at T=950°C is shown in Figure 4. Deformation at σ=301 MPa (Fig. 4a) leads to the formation of the γ/γ'-raft structure. Stereo imaging shows that the γ'-rafts are cut by dislocations. The dislocation networks at the γ/γ'-interfaces are not planar and do not penetrate into the γ'-phase. For high stresses (σ≥512 MPa) the creep life was too short for the raft structure to develop (Fig. 4b). Again, dense dislocation networks are located at the γ/γ' interface, in particular perpendicular to the stress axis. These results are in agreement with other findings on the creep deformation of monocrystal superalloys, cf. for example [13]. In contrast to deformation of SRR 99 at T=900°C [6, 7], stacking faults can be identified clearly within the γ'-precipitates.

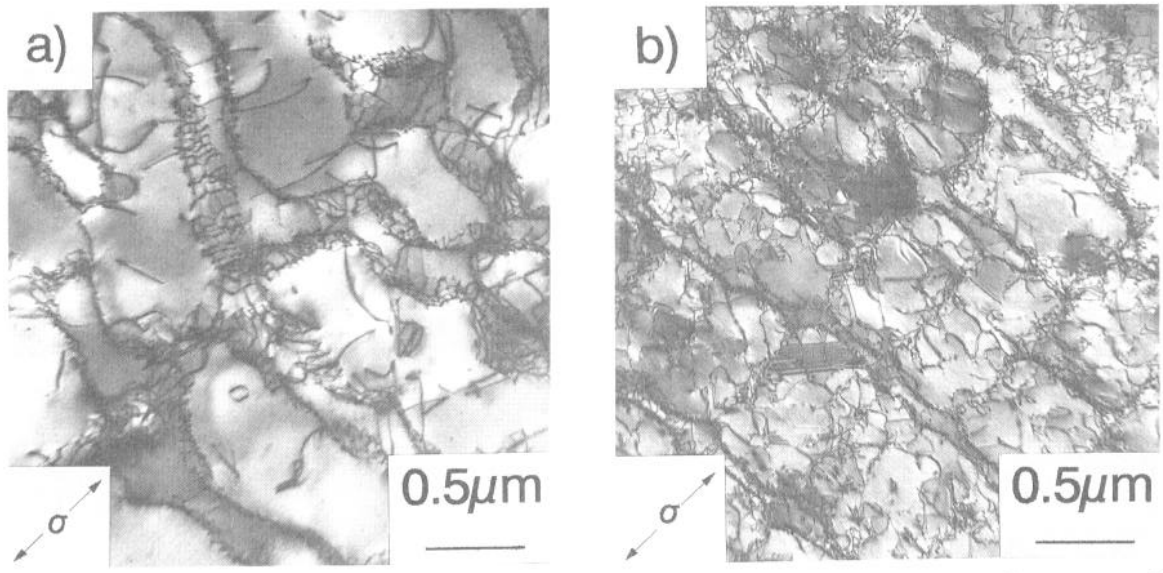

Figure 4: TEM micrographs showing the typical dislocation microstructures after creep till rupture at T=950°C. (a) σ=301 MPa. (b) σ=654 MPa. (100) foils, parallel to stress axis [001].

Stress Exponent, Stress-Change-Tests

The stress dependence of the steady-state creep rate $\dot{\varepsilon}_{ss}$ is usually described by a power law:

$$\dot{\varepsilon}_{ss} = A_1 \cdot \sigma^n \cdot \exp\left(-\frac{Q}{kT}\right) \quad (1)$$

where A_1 is a constant, σ the applied stress, n the stress exponent, Q the activation energy, k the Boltzmann constant and T the absolute temperature. Like many technical materials, the alloy CMSX-4 does not exhibit a real steady-state creep rate. Rather, as discussed, a minimum creep rate $\dot{\varepsilon}_{min}$ is observed which is used here instead of the steady-state creep rate. The determination of the stress exponent yields for T=800°C and T=950°C the values n=13.5 and n=8.8, respectively. Creep curves at T=800°C show two minimum creep rates. Consequently, at T=800°C two different n-values are obtained. The stress exponent n=13.5 belongs to the absolute minimum of the creep rate at higher strains. In the case of the $\dot{\varepsilon}_{min}$-value observed after a very small plastic strain, a smaller stress exponent n=9.5 is found. Figure 5 shows stress-change tests for T=950°C between an upper stress of 512 MPa and a lower stress of 406 MPa and the monotonic curves for both stresses. The stress exponent, defined as $n = \Delta(\ln\dot{\varepsilon})/\Delta(\ln\sigma)$, decreases from ca. 7.5 to ca. 5.8 with increasing strain. The stress exponent determined by stress-change tests was always lower than that obtained from the evaluation of the minimum creep rates. It should be noted that these stress changes correspond in good approximation to tests at constant microstructure. Hence, the stress exponents determined from stress-change tests are considered to be more reliable than those determined from minimum creep rates measured for not identical microstructures. In either case, the stress exponents are unrealistically high and difficult to interpret.

In Fig. 5a the stress first applied was 406 MPa, whereas in Fig. 5b the test started with σ= 512 MPa. It is evident from Fig. 5 that creep after the first stress change proceeds at a higher (lower) creep rate compared to the monotonic curves, when the first deformation is performed at the lower (higher) stress level. From the comparison of the time required for a certain strain, it is concluded that merely time-dependent processes cannot cause such behaviour. Rather, dynamic processes, strain- or stress-enhanced, must be responsible for the creep acceleration observed in these stress-change tests.

The formation of the γ/γ'-raft structure could be such a dynamic process. This conclusion which reflects a deterioration of creep properties due to the formation of the γ/γ'-raft struc-

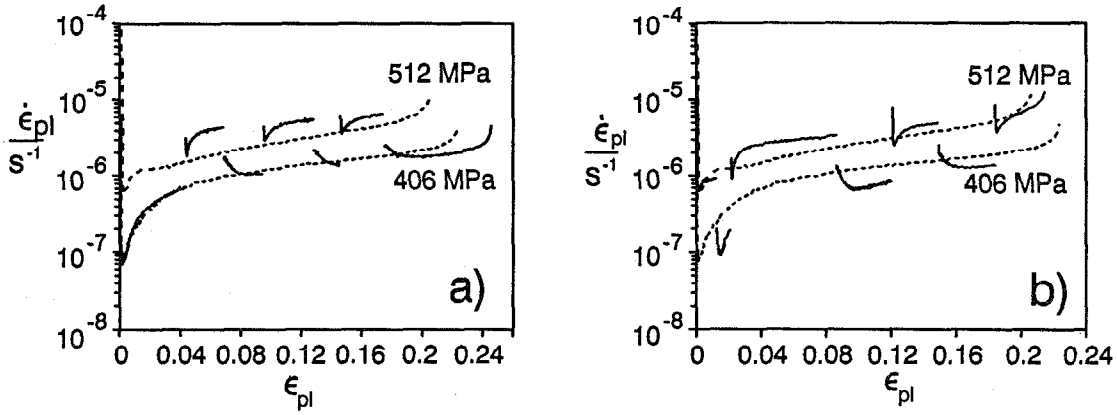

Figure 5: Stress-change tests at T=950°C between σ=406 MPa and σ=512 MPa and monotonic creep curves corresponding to σ=406 MPa and σ=512 MPa, respectively. (a) Test started with the lower stress σ=406 MPa. (b) Test started with the higher stress σ=512 MPa.

ture, is also supported by a comparison of the microstructure prevailing prior to the first stress change. In Fig. 5a, during the first deformation at σ= 406 MPa, enough time was available to allow the γ/γ'-raft structure to develop prior to the first stress change, whereas in Fig. 5b the first deformation at σ= 512 MPa was too rapid for the raft structure to develop. Therefore, it can be concluded that, in the case described, the raft structure led to a deterioration of the creep strength, as reflected in an increase of the creep rate, under the given conditions. This conclusion is in agreement with the results of previous investigations on SRR 99 [6, 7].

Particle Hardening, Threshold Stress Concept

In the case of alloys hardened by second-phase particles another equation, based on the assumption that the deformation requires an additional particle stress σ_p compared to the deformation of the particle-free matrix, was proposed to describe the creep behaviour [17]:

$$\dot{\varepsilon}_{ss} = A_2 \cdot (\sigma - \sigma_p(\sigma))^{n_m} \cdot \exp\left(-\frac{Q_{SD}}{kT}\right) \qquad (2)$$

In eq.(2) A_2 is a constant, σ_p is the stress-dependent threshold stress due to the particles, n_m is the stress exponent of the matrix and Q_{SD} the activation energy for self diffusion. Thus the creep behaviour of the two-phase alloy can be described by the behaviour of the matrix. In the limit of vanishing σ_p, eq.(2) approaches eq.(1).
The threshold stress can be determined by plotting the data in a Lagneborg-Bergman diagram [17] and by applying a procedure introduced by Reppich and co-workers [18]. Figure 6a shows the determination of the threshold stress σ_p according to [18]. The value of σ_p is obtained as the difference between the stresses which are needed to deform Nimonic 75, considered as representative of the matrix material, and CMSX-4 at the same creep rate. In contrast to the earlier study on SRR 99 [7], the creep behaviour of the particle-free matrix material Nimonic 75 was described by a hyberbolic sine law which resulted in a stress-dependent instead of a constant stress exponent. It must be noted, however, that whereas Nimonic 75 can be considered as a good approximation to the matrix material in SRR 99, this assumption is less justified for the Rhenium-containing alloy CMSX-4.
In Fig. 6b the obtained values of σ_p are plotted as a function of stress. Up to high stresses, σ_p is a linear function of the applied stress. At very high stresses, σ_p shows significant deviations from linearity which presumably correspond to a change in the deformation mechanism. It can be seen that in this representation, at 800°C and 950°C, CMSX-4 possesses higher σ_p-values than SRR 99 at 750°C and 900°C, respectively. However this result may be caused by differences in the matrix composition of the two alloys.

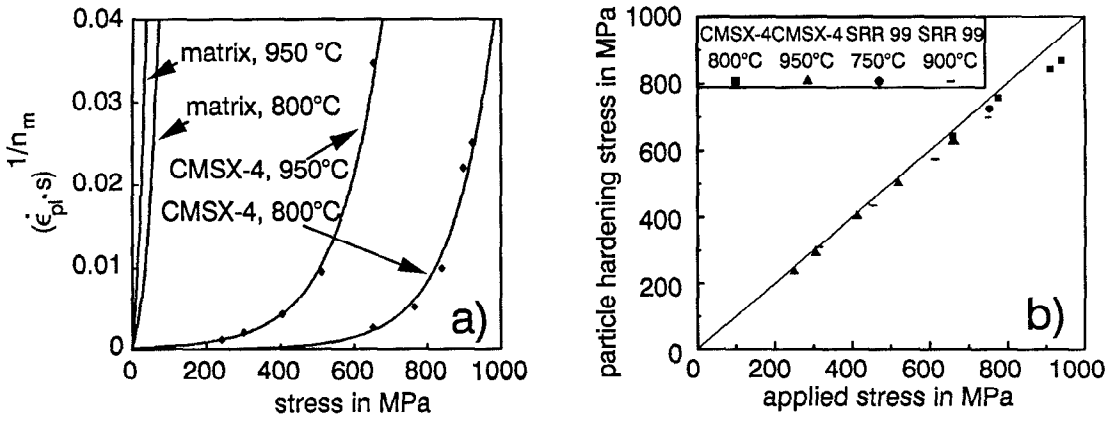

Figure 6: (a) Lagneborg-Bergman diagram for T=800°C and T=950°C. (b) stress dependence of the threshold stress σ_p for CMSX-4 and SRR 99. The straight line represents $\sigma=\sigma_p$.

Creep Rupture Diagrams

In Fig. 7 the standard-type creep-rupture diagram is shown for the alloy CMSX-4. Besides the rupture data the values for 1%, 2%, 3% and 5% plastic strain are also included. It is evident that all curves show a curvature. Therefore the extrapolation to long times is associated with great uncertainty. For SRR 99 a similar diagram is obtained.

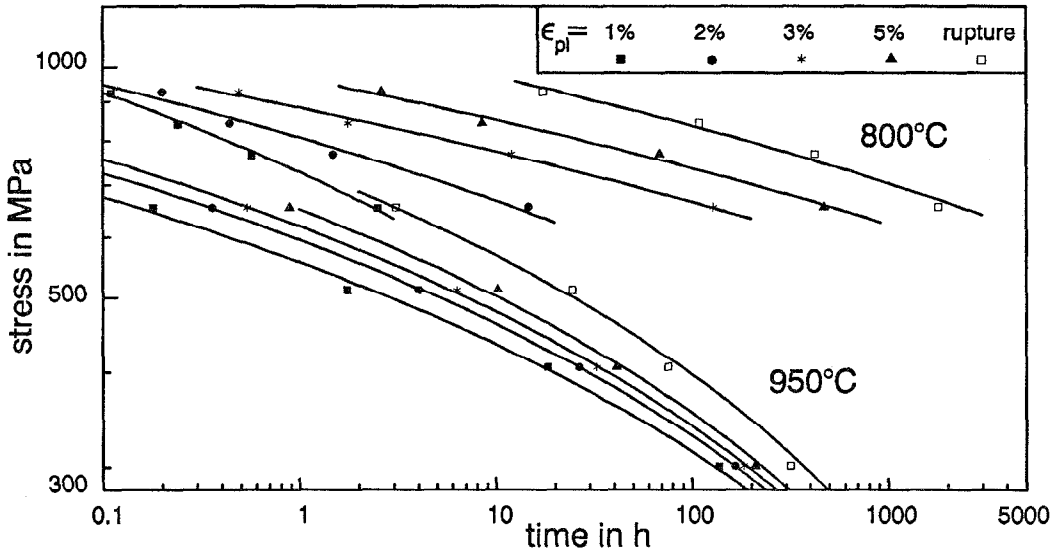

Figure 7: Standard creep rupture diagram for T=800°C and T=950°C for the alloy CMSX-4.

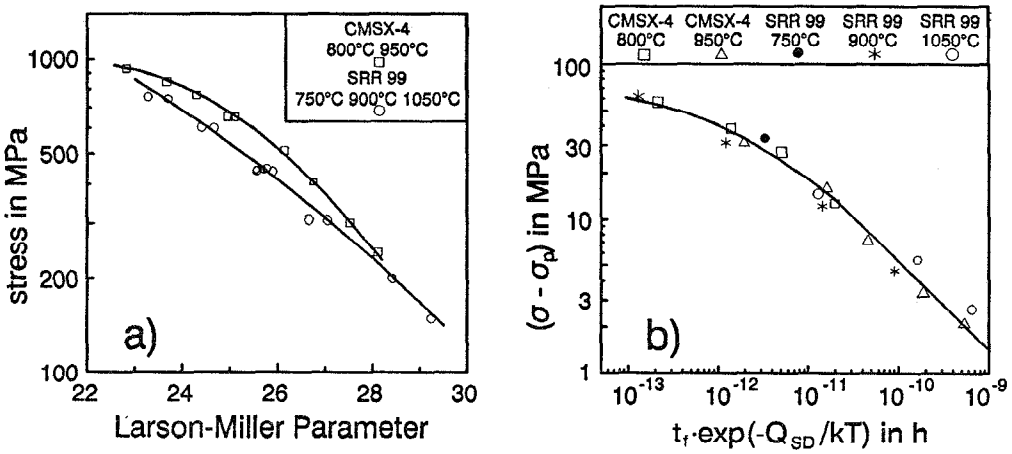

Figure 8: (a) Temperature-compensated Larson-Miller plot. (b) Modified creep-rupture diagram based on the threshold stress concept with data from tests on CMSX-4 and SRR 99.

In order to compare the creep-rupture properties of CMSX-4 and SRR 99, it is expedient to choose a representation as a function of a temperature-compensated time. Fig. 8a shows a Larson-Miller plot of the stress-rupture data of CMSX-4 and SRR 99 for five different temperatures. The Larson-Miller Parameter represents a temperature-compensated life time. It is evident that the data of CMSX-4 lie above the curve corresponding to SRR 99. The horizontal distance between the two curves represents the temperature advantage of CMSX-4. Accor-

ding to this plot, the alloy CMSX-4 offers an improved creep temperature capability of about 20°C at low stresses and more than 40°C at higher stresses.
With the obtained σ_p-values, it is possible to describe the creep-rupture behaviour in the framework of the modified threshold stress concept [18]. Knowing the specific $\sigma_p(\sigma)$-value for a certain stress and temperature, the creep-rupture strength of two-phase materials can be described through the creep-rupture strength of the particle-free matrix material [7]. Figure 8b shows this modified creep-rupture strength diagram, based on the threshold stress concept. It is gratifying to note that all creep-rupture data of SRR 99 and CMSX-4 obtained at different temperatures and stresses fall on one common curve. In the earlier work on SRR 99, a constant value of n_m was used and, consequently, a common straight line was obtained [6, 7]. In either case, the results confirm that the approach based on the threshold stress concept is self-consistent. Nonetheless, it would be desirable to understand better the physical nature of the particle stress σ_p and to develop models which allow its calculation.

Conclusions

The most important conclusions drawn from this study on the creep behaviour of CMSX-4 single crystals are as follows:

a) The creep curves of CMSX-4 exhibit no steady-state creep regime. In all cases, investigated so far, the creep rate goes through a minimum (or even two minima) and then increases continuously till fracture.
b) Creep curves plotted in the form of (plastic) creep rate $\dot{\varepsilon}_{pl}$ versus (plastic) strain ε_{pl} provide more information than the more common plots of (plastic) strain ε_{pl} versus time t.
c) At the temperature T=800°C two minimum creep rates are observed. No morphological changes of the γ'-particles occurred during creep for stresses $\sigma \geq 654$ MPa.
d) At the temperature T=950°C the minimum creep rate $\dot{\varepsilon}_{min}$ appears after very small strains. For stresses $\sigma \leq 406$ MPa γ'-rafts form which are aligned normal to the stress axis.
e) The increase of $\dot{\varepsilon}_{pl}$ immediately after $\dot{\varepsilon}_{min}$ is attained is more pronounced for low stresses, due to the formation of the γ/γ'-raft structure, accompanied by a deterioration of the creep properties.
f) The creep-rupture behaviour of both CMSX-4 and SRR 99 can be described in a modified creep-rupture diagram, based on the threshold stress concept.
g) According to a Larson-Miller plot, the alloy CMSX-4 offers an improved creep temperature capability, compared to SRR 99, of about 20°C at low stresses and more than 40°C at higher stresses.

Acknowledgments
The financial support of this work by the Bundesminister der Verteidigung under research contract number T/RF45/L0010/L1417 is acknowledged gratefully.

References

[1] P. Caron et al., "Creep Deformation Anisotropy In Single Crystal Superalloys", in 'Superalloys 1988', (eds. D. N. Duhl, G. Maurer, S. Antolovich, C. Lund and S. Reichman), The Metall. Soc., Warrendale, Pennsylvania (1988), 215-224.

[2] A. D. Cetel and D. N. Duhl, "Second-Generation Nickel-Base Single Crystal Superalloy", in 'Superalloys 1988', (eds. D. N. Duhl, G. Maurer, S. Antolovich, C. Lund and S. Reichman), The Metall. Soc., Warrendale, Pennsylvania (1988), 235-244.

[3] A. F. Giamei and D. L. Anton, "Rhenium Additions to a Nickel-Base Superalloy: Effects on Microstructure", Met. Trans., 16A (1985), 1997-2005.

[4] D. Blavette, P. Caron and T. Khan, "An Atom-Probe Study of Some Fine-Scale Micro-

structural Features in Ni-Based Single Crystal Superalloys", in 'Superalloys 1988', (eds. D. N. Duhl, G. Maurer, S. Antolovich, C. Lund and S. Reichman), The Metall. Soc., Warrendale, Pennsylvania (1988), 305-314.

[5] S. M. Foster, T. A. Nielsen and P. Nagy, "Enhanced Rupture Properties in Advanced Single Crystal Alloys", in 'Superalloys 1988', (eds. D. N. Duhl, G. Maurer, S. Antolovich, C. Lund and S. Reichman), The Metall. Soc., Warrendale, Pennsylvania (1988), 245-254.

[6] J. Hammer, Doctorate Thesis, Universität Erlangen-Nürnberg, (1990).

[7] J. Hammer and H. Mughrabi, "High Temperature Creep and Microstructure of the Monocrystalline Nickel-Base Superalloy SRR 99", in 'Advanced Materials and Processes, Proc. of the First European Conf. on Advanced Materials and Processes', Aachen, Germany (edited by H. E. Exner and V. Schumacher), Vol. 1: Advanced Processing and High Temperature Materials (co-edited by D. Driver and H. Mughrabi), DGM Informationsgesellschaft, Oberursel (1990), 445-450; and unpublished work.

[8] T. M. Pollock and A. S. Argon, "Creep Resistance of CMSX-3 Nickel Base Superalloy Single Crystals", Acta metall. et mater., 40 (1992), 1-30.

[9] H.-A. Kuhn and H. G. Sockel, "Contributions of the Different Phases of Two NickelBase Superalloys to the Elastic Behaviour in a Wide Temperature Range", phys. stat. sol. (a), 119 (1990), 93-105.

[10] W. Blum and B. Ilschner, "Über das Kriechverhalten von NaCl-Einkristallen", phys. stat. sol., 20 (1967), 629-642.

[11] M. V. Nathal and L. J. Ebert, "The Influence of Cobalt, Tantalum and Tungsten on the Elevated Temperature Mechanical Properties of Single Crystal Nickel-Base Superalloys", Met. Trans., 16A (1985), 1863-1870.

[12] B. F. Dyson and M. McLean, "Particle-Coarsening, σ_0 and Tertiary Creep", Acta metall., 31 (1983), 17-27.

[13] M. Feller-Kniepmeier and T. Link, "Correlation of Microstructure and Creep Stages in the ⟨100⟩ Oriented Superalloy SRR 99 at 1253 K", Met. Trans., 20A (1989) 1223-1238.

[14] H.-A. Kuhn et al., "An X-Ray Study of Creep-Deformation Induced Changes of the Lattice Mismatch in the γ'-Hardened Monocrystalline Nickel-Base Superalloy SRR 99", Acta metall. et mater., 39 (1991), 2783-2794.

[15] T. L. Lin and Mao Wen, "The Deformation Mechanism of a γ' Precipitation-Hardened Nickel-Base Superalloy", Mater. Sci. Eng., A128 (1990), 23-31.

[16] M. V. Nathal, R. A. MacKay and R. V. Miner, "Influence of Precipitate Morphology on Intermediate Temperature Creep Properties of a Nickel-Base Superalloy Single Cystal", Met. Trans., 20A (1989), 133-141.

[17] R. Lagneborg and B. Bergman, "The Stress/Creep Rate Behaviour of Precipitation-Hardened Alloys", Met. Sci., 10 (1976), 20-28.

[18] B. Reppich et al., "Microstructural Modelling of The Creep Behaviour of Particle-Strengthened Superalloys", steel research, 61 (1990), 251-257.